An Evaluation of Earthquake Damage Scales used in Remote Sensing Studies of the 2003 Bam, Iran Earthquake

Ellen M. Rathje[1] and Beverley J. Adams[2]

Introduction

The 2003 Bam, Iran earthquake provided an excellent opportunity to demonstrate the different approaches for earthquake damage detection using remote sensing, as well as the resulting damage scales used to quantify damage. A multitude of pre- and post-earthquake remote sensing data was available for this earthquake and was analyzed by various research groups from around the world. The 2005 special issue of the journal Earthquake Spectra dedicated to the Bam earthquake included eleven papers on the use of remote sensing to assess the damage patterns in the city of Bam. This paper describes the different approaches to damage detection presented in these papers (pixel-based vs. object-based, image analysis vs. visual analysis), and compares the damage scales and resulting damage patterns.

Damage Scales

The 2003 Bam, Iran earthquake provides an excellent opportunity to demonstrate the different approaches for earthquake damage detection using remote sensing. A multitude of pre- and post-earthquake remote sensing data was available (HR optical, MR optical, LR SAR), and these data were analyzed by various researchers from around the world. The 2005 special issue of the journal *Earthquake Spectra* dedicated to the Bam earthquake included eleven papers on the use of remote sensing to assess damage patterns. Figure 1 summarizes the approaches used by the contributors to this special issue.

The approaches to earthquake damage detection can be generally divided into two main categories: pixel-based analyses and object-based analyses. In pixel-based analysis, each pixel is assigned a separate damage state based on the characteristics of the pixel. While some contextual information from adjacent pixels (e.g., texture, edges) may also be used in assigning the damage state, each pixel is assigned a separate level of damage. Often, adjacent pixels are then aggregated to assign an average damage level to an area. In object-based analysis, the original pixels are first segmented into objects and all subsequent analyses are performed on, and damage levels are assigned to, each object as a whole. Because the size of the objects of interest are relatively small in earthquake damage detection (e.g., buildings), object-based analysis generally requires the use of HR imagery.

Within the context of pixel or object-based analyses, researchers may use either image analysis or visual analysis to identify damage. In general, lower resolution data and pixel-based approaches require some form of computer-based image analysis because the urban infrastructure is not visually identifiable within the LR/MR imagery or within a single pixel. The computer-based analytical techniques generally fall into two categories: those that use pre- and post-earthquake data to identify change (i.e., change detection, with all change ascribed to earthquake damage), and those that only use post-earthquake imagery to identify damage (i.e., thematic classification). For HR data, either image analysis (change detection or thematic classification) or visual analysis can be performed.

The details of the specific algorithms used for image analysis vary widely and depend on various factors, such as the type of remote sensing data (optical vs. SAR), its resolution, availability of pre- and post-event data. The analytical details will not be discussed here, but a good overview of the available algorithms can be found in the papers listed in Figure 1. When using image analysis to identify earthquake damage, it is important to realize that the specific procedures, criteria, thresholds, etc. that successfully identify damage for one earthquake, may not be as successful for another. This issue was identified by Matsuoka and Yamazaki (2005) when they tried to apply the SAR damage identification algorithms developed from the Kobe earthquake in Japan to SAR data from the Bam earthquake. The different structural types (larger engineered structures in Kobe vs. smaller non-engineered adobe

[1] University of Texas at Austin, 1 University Station, C1792, Austin, TX 78712. E-mail:e.rathje@mail.utexas.edu
[2] Imagecat, Inc., European Operations, Ashtead, Surrey, KT21 2BT, UK. E-mail: bja@imagecatinc.com

structures in Bam) precluded direct application of the original algorithm and resulted in a modified algorithm for the Bam earthquake. For visual analysis, the criteria for damage identification are more subjective and the results depend on the experience of the analyst (Saito et al. 2005). For all approaches, the raw damage identification results generally are used within the framework of a damage scale. To date, various damage scales have been developed by different researchers for different types of remote sensing data. The damage scales used in the studies of the Bam, Iran earthquake, as presented in the 2005 EERI Special Issue, are summarized in Table 1.

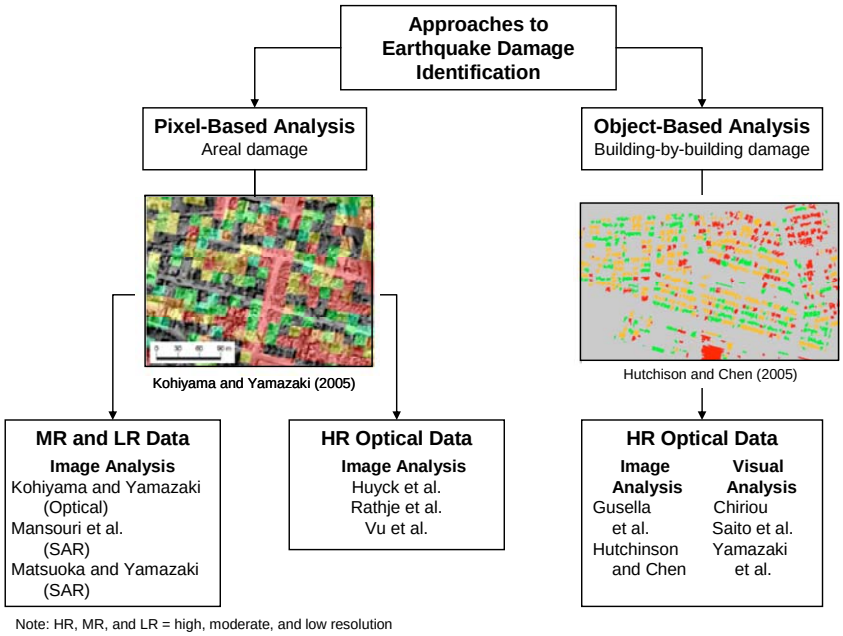

Fig. 1. Approaches to earthquake damage identification used in studies of the Bam earthquake

The damage scales used for pixel-based analyses are quite distinct from those used in object-based analyses. The pixel-based approaches typically define damage based on either the damage intensity of a single pixel or within a windowed area measuring *n* by *n* pixels. The damage scales that utilize data from only a single pixel are typically applied to LR or MR data because each pixel represents a relatively large dimension (> 10 m). Averaging damage within a window is generally used for pixel-based approaches applied to HR imagery, because there are often spurious single pixels, or small groups of pixels, that are identified as damage but that are not damage. These misidentified pixels may represent pixels that simply look like damage or they may represent non-earthquake change (e.g., seasonal vegetation changes). By averaging damage within a window or by looking at the percentage of damage pixels within a window, the misidentified pixels can be essentially filtered out or de-emphasized, which results in a damage map that represents significant and important damage. Nonetheless, large areas of non-earthquake change (e.g., new development along the edge of an urban area) may still be identified as significant earthquake damage.

Table 1. Damage Scales used in Remote Sensing Studies of the Bam, Iran Earthquake

	Damage Scale	Appropriate Data Types	Examples from Studies of Bam Earthquake
Pixel-based Approaches	Damage intensity of a single pixel	MR or LR Optical or SAR	Kohiyama and Yamazaki (2005) Mansouri et al. (2005) Matsuoka and Yamazaki (2005)
	Percentage of damaged pixels or average damage state within a window	HR Optical	Huyck et al. (2005) Mansouri et al. (2005) Rathje et al. (2005) Vu et al (2005)
Object-based Approaches	Identify collapsed building	HR Optical	Gusella et al. (2005)
	Identify damage grade of each building	HR Optical	Hutchinson and Chen (2005) Yamazaki et al. (2005)
	Number or percentage of collapsed buildings within a region	HR Optical	Chiriou (2005) Saito et al. (2005)

The damage scales used with object-based approaches generally focus on assigning damage on a building-by-building basis (Table 1). Each structure may be assigned to a binary classification of collapsed vs. non-collapsed, or assigned a specific damage grade based on standard scales used in field reconnaissance (e.g., European Macroseismic Scale, EMS). The EMS damage grades are G5-destruction, G4-very heavy damage, G3-substantial damage, G2-moderate damage, and G1-slight to negligible damage. In general it is difficult to distinguish between all of these damage grades, with the most success coming in identifying G4 and G5 (Hutchinson and Chen 2005, Yamazaki et al. 2005). To aggregate the building-by-building information, the number or percentage of collapsed buildings within a region or district may also be reported.

Assessment of Damage Scales

Quantitative assessment of the different damage scales is difficult. Figure 2 presents examples from the Bam earthquake of the damage data derived using the five damage scales listed in Table 1. A qualitative comparison between each image reveals that they consistently identify that the damage was concentrated in the eastern sections of the city, with the most intense damage occurring in the north-east and south-east. This consistency in general damage patterns is encouraging and provides confidence in using these types of damage estimates for rapid post-earthquake activities. However, it is difficult to quantitatively evaluate and compare there different damage assessments.

Using damage estimates from remote sensing in more detailed, long-term earthquake studies requires a more quantitative assessment of their accuracy. Yamazaki et al. (2005) compared the EMS damage grades derived from visual analysis of HR imagery with those assigned by the field reconnaissance of Hisada et al. (2005). Over four hundred buildings were compared and an error matrix comparing the results was developed (Table 3). The accurately identified structures are shaded on the diagonal and represent an overall accuracy of 52.8%. The differences between the field survey and remote sensing survey can be quantified via commission error, defined as the percentage of structures incorrectly assigned to each damage grade, and omission error, defined as the percentage of structures incorrectly omitted from each damage grade (Lillesand et al. 2004). Considering the errors for individual damage grades, G5 shows the smallest errors with only 15% commission error and 38% omission error. However, the commission and omission errors for the other damage grades are significant, particularly for G4, which has a commission error of 79.2% (i.e., 79.2% of the buildings identified as G4 were *not* G4) and an omission error of 82.5% (i.e., 82.5% of the actual G4 buildings were assigned other grade levels). These results indicate that it is difficult to distinguish moderate to heavy damage levels. Additionally, by

comparing the total number of buildings in the heaviest damage grades from each survey (165 for remote sensing vs. 215 for field survey) it appears that the remote sensing observations underestimate the numbers of heavily damaged buildings. This result is due to the fact that heavy damage may not be visible from the aerial view of the remote sensing data.

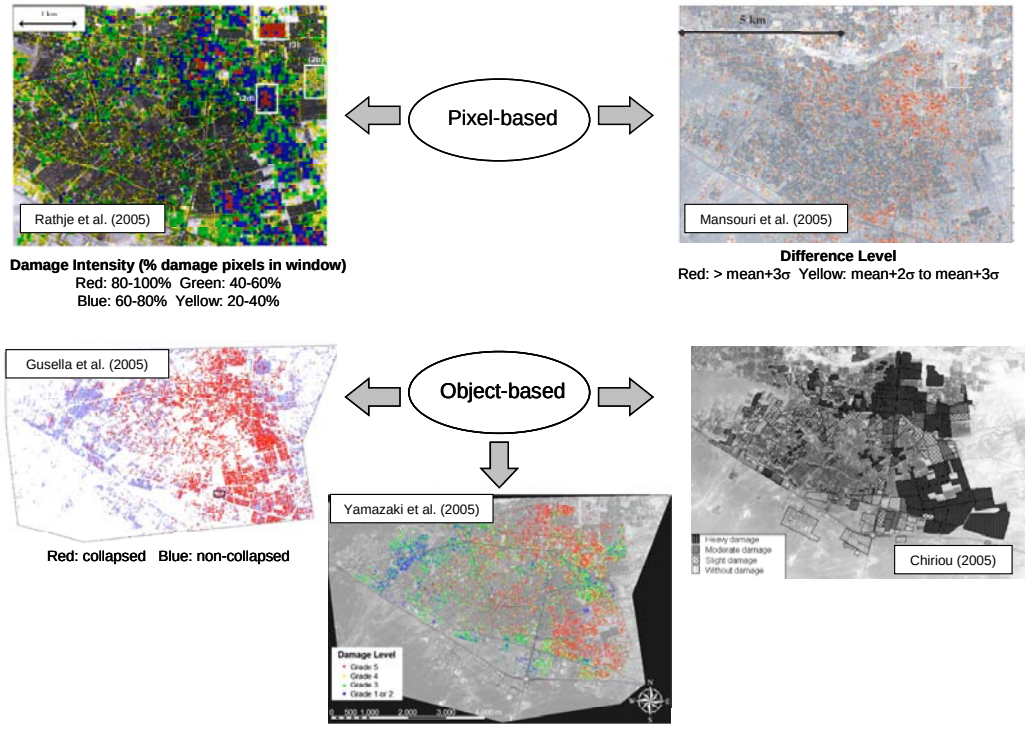

Figure 2. Examples of the damage products for the Bam, Iran earthquake derived from remote sensing data and using the five types of damage scales listed in Table 1.

Table 2. Error matrix for damage study of Bam earthquake (after Yamazaki et al. 2005)

		Field Survey					
		G1 & 2	**G3**	**G4**	**G5**	**SUM**	**Commission Error (%)**
Remote Sensing Survey	**G1 & 2**	62	29	15	2	108	*42.6*
	G3	41	57	30	25	153	*62.7*
	G4	2	10	11	30	53	*79.2*
	G5	0	10	7	95	112	*15.2*
	SUM	105	106	63	152	426	--
	Omission Error (%)	*41.0*	*46.2*	*82.5*	*37.5*	--	**Overall Acc** 225/426 = *52.8%*

Table 3. Condensed error matrices for Yamazaki et al. (2005) damage study

		Field Survey				
		G1 & 2	**G3**	**G4 &5**	**SUM**	**Commission Error (%)**
Remote Sensing Survey	**G1 & 2**	62	29	17	108	*42.6*
	G3	41	57	55	153	*62.7*
	G4 &5	2	20	143	165	*13.3*
	SUM	105	106	215	426	--
	Omission Error (%)	*41.0*	*46.2*	*33.5*	--	**Overall Acc** 262/426 = *61.5%*

		Field Survey			
		G1 to 3	**G4 &5**	**SUM**	**Commission Error (%)**
Remote Sensing Survey	**G1 to 3**	189	72	261	*27.6*
	G4 &5	22	143	165	*13.3*
	SUM	211	215	426	--
	Omission Error (%)	*10.4*	*33.5*	--	**Overall Acc** *77.9%*

		Field Survey			
		G1 to 4	**G5**	**SUM**	**Commission Error (%)**
Remote Sensing Survey	**G1 to 4**	257	57	314	*18.2*
	G5	17	95	112	*15.2*
	SUM	274	152	426	--
	Omission Error (%)	*6.2*	*37.5*	--	**Overall Acc** *82.6%*

The error matrix in Table 2 can be condensed to consider which damage grades can be most accurately distinguished from high resolution imagery (Table 3). If G4 and G5 are combined into a single category, the overall accuracy increases to 61.5%, but the commission errors for the lower grades remain the same (Table 3). If the data are combined such that only binary grades exist (G1 to 3 vs. G4 to 5 or G1 to 4 vs. G5), the overall accuracies increase to around 80%, and most of the commission and omission errors are less than 30% (Table 3). For either case, the largest error is the omission error for the largest damage grade (~35%), which again indicates that the remote sensing observations tend to underestimate damage.

Most of the other studies from the Bam, Iran earthquake assessed the accuracy of their results through a qualitative comparison with a damage map prepared by the Geological Survey of Iran (GSI). The damage scale used by the GSI is based on the percentage of collapsed buildings as identified from aerial

photographs. The comparisons between the remote sensing results (e.g., Figure 2) and the GSI map were generally favorable; however, because the GSI map was derived from aerial photos it cannot be considered ground truth.

Conclusions

Various remote sensing damage scales have been proposed and used to evaluate damage patterns from earthquakes. This paper summarized the approaches to damage identification and the damage scales used to quantify damage from the 2003 Bam, Iran earthquake. Either pixel-based or object-based approaches have been used. General damage patterns from the various approaches agree well with field observations. However, only object-based approaches can develop building-by-building damage estimates. Compared with detailed field studies, the object-based approaches work best when trying only to distinguish the most heavily damaged buildings.

References

Chiriou, L., 2005, Damage assessment of the 2003 Bam, Iran earthquake using Ikonos imagery, *Earthquake Spectra*, 21(S1), S219-S224.

Gusella, L., Adams, B., Bitelli, G., Huyck, C., and Mognol, A., 2005, Object-oriented understanding and post-earthquake damage assessment for the 2003 Bam, Iran earthquake, *Earthquake Spectra*, Earthquake Engineering Research Institute, 21(S1), S225-S238.

Hisada, Y., Shibayama, A., and Ghayamghamian, M. R., 2005. Building damage and seismic intensity in Bam City from the 2003 Iran, Bam, Earthquake, *Bull. Earthquake Res. Inst., Univ. Tokyo* **79** (3 & 4), 81-94.

Hutchinson, T., and Chen, Z., 2005, Optimized estimated ground truth for object-based urban damage estimation using satellite images from the 2003 Bam, Iran earthquake, *Earthquake Spectra*, 21(S1), S239-S254.

Huyck, C., Adams, B., Cho, S., Chung, H.-C., and Eguchi, R., 2005, Towards rapid citywide damage mapping using neighborhood edge dissimilarities in very high-resolution optical satellite imagery-application to the 2003 Bam, Iran earthquake, *Earthquake Spectra*, 21(S1), S255-S266.

Kohiyama, M., and Yamazaki, F., 2005, Damage detection for 2003 Bam, Iran earthquake using Terra-ASTER satellite imagery, *Earthquake Spectra*, 21(S1), S267-S274.

Lillesand, T.M., Kiefer, R.W., and Chipman, J.W. 2004, *Remote Sensing and Image Interpretation.* 5th Edition, Wiley and Sons, New York.

Mansouri, B., Shinozuka, M., Huyck, C., and Houshmand, B., 2005, Earthquake-induced change detection in the 2003 Bam, Iran earthquake by complex analysis using Envisat ASAR data, *Earthquake Spectra*, 21(S1), S275-S284.

Matsuoka, M. and Yamazaki, F., 2005, Building damage mapping of the 2003 Bam, Iran earthquake using Envisat/ASAR intensity imagery, *Earthquake Spectra*, 21(S1), S285-S294.

Rathje, E.M., Crawford, M., Woo, K., and Neuenschwander, A. 2005. Damage Patterns from Satellite Images from the 2003 Bam, Iran Earthquake, *Earthquake Spectra*, 21(S1), S295-307.

Saito, K., Spence, R., and Foley, T., 2005, Visual damage assessment using high-resolution satellite images following the 2003 Bam, Iran earthquake, *Earthquake Spectra*, 21(S1), S309-S318.

Vu, T., Matsuoka, M., and Yamazaki, F., 2005, Detection and animation of damage using very high-resolution satellite data following the 2003 Bam, Iran earthquake, *Earthquake Spectra*, 21(S1), S319-S327.

Yamazaki, F., Yano, Y., and Matsuoka, M., 2005, Visual damage interpretation of buildings in Bam city using Quickbird images following the 2003 Bam, Iran earthquake, *Earthquake Spectra*, 21(S1), S329-S336.